Modelling and Analysis of Load Frequency Control in Small Power Systems: a Case Study of New Zealand Network

Pedro Ferreira Gutman, Peter Makolo and Ramon Zamora
Department of Electrical and Electronic Engineering
Auckland University of Technology – AUT
Auckland, New Zealand
ramon.zamora@aut.ac.nz

***Abstract*—Some challenges experienced by small power systems are escalating as penetration of renewable energy sources (RESs) increases. To overcome the challenges related to frequency stability, this paper discusses about a load frequency control model that can respond to an emulation of a real operation. The inclusion of energy storage systems to the model to support frequency control in a low inertia condition is also addressed. The increase of RES penetration is simulated by a decrease in the system inertia constant. To compensate for the low inertia and to improve the frequency response of the system, a virtual inertia is installed. The proposed load frequency control model is implemented in Matlab/Simulink. The multiple frequency keeping (MFK) ancillary service and the frequency keeping control (FKC) are included in the proposed model. The proposed model is simulated in a New Zealand power system as a case study for small networks. The simulation results verified that the developed model works as expected.**

Keywords— Virtual/Synthetic Inertia, multiple frequency keeping, frequency keeping control, frequency response, RoCoF

I. INTRODUCTION

The frequency of a power system remains constant and stable provided there is a balance between electrical power supply and power demand plus losses [1]. To maintain this balance and hence frequency stability in power grids, power system controls are required. Power system controls have a purpose of preserving system integrity and restore normal operation following a disturbance [2]. As many other small networks, New Zealand power system is susceptible to frequency deviations. Large frequency disruptions can damage equipment and cause overload in transmission lines that can lead to a cascade failure in the power system and entail power outages. Therefore, unlike huge and roust power networks, a reliable frequency control approach for small power systems is extremely important.

The generation sector in New Zealand, as case study for this research, contains a mix of hydro, thermal, geothermal, wind, coal and gas power plants. An average of 80% of this generation comes from renewable sources (RESs) and the government intends to increase the RESs share to 100% by the end of 2035 [3]. The actual installed solar panels in NZ are mainly residential and has been increasing steadily mostly due to the decrease in its cost and incentive of its usage by electricity distributors. The wind generation has also increased, with a forecast of around 20% of New Zealand's installation capacity by the year 2035 [4]. However, the challenges that are associated with these RESs to the stability of the network cannot be underestimated. As these types of generation works differently from conventional synchronous generators such as hydro and thermal plants, it has a direct impact on the stability of the power system. Due to the actual small installed capacity of solar panels – 75MW [5] and wind generation – 658MW [6] currently, the impact to the network stability is not significant yet. However, the future high penetration plans for these RESs will significantly influence the system frequency response.

High level of non-dispatchable RESs such as wind and solar in small networks will cause the overall decrease in effective inertia constant of the system. The main reason behind this inertia decrease is the fact that non-dispatchable RESs are connected to the grid through inverters. In this way, the inertia from wind turbines and blades are decoupled from the grid and therefore contribute zero inertia to the network. This situation leads to an increase in the rate of change of frequency (RoCoF) for any disturbance in power system. Consequently, it becomes more difficult for the system to restore the frequency to normal values. In worst cases, the frequency is not restored, which can lead to power outages due to the activation of protection relays. Therefore, small networks such as New Zealand's grid must be prepared to face the challenges related to high penetration of RESs.

To avoid bigger system disturbances and/or mal-operation due to frequency disruption in a future scenario, this research work proposes a load frequency control technique. The proposed technique will manage frequency response and maintain frequency stability in small networks such as New Zealand. The technique incorporates the usage of a virtual inertia control to deal with the high penetration of RES and thus the decrease in overall inertia. The derivative control block-based topology has been used to emulate the inertia of synchronous generators. The distributed generation is connected to a DC bus through an inverter, which in turn is connected to the AC grid. The inverter can be used with control algorithms and energy storage system (ESS) to provide the virtual/synthetic inertia. This approach has shown good results for small power systems.

The rest of the paper is structured as follows: Section II introduces the theoretical background and formulation of the problem under discussion of this research work. Methodology and model for load frequency control are described in section III. Section IV presents simulations for the New Zealand's developed model. Section V presents and discusses the results

of the simulations generated. Finally, conclusion and future research work are presented in section VI.

II. THEORETICAL BACKGROUND AND CONCEPTS

A. Frequency Management

With the purpose of maintaining the frequency stability, the power system has several frequency mitigation measurements that are used for different types of situations. For an under-frequency event, there are two types of risks, which are contingent event (CE) and extended contingent event (ECE). The ECE is a less probable event. Thus, the protection relies mainly on the automatic under frequency load shedding (AUFLS) [7]. The CE represents an event of disconnection of a single power system component, such as a generator or a transmission circuit and are more likely to happen. As a solution, the system operator can purchase generating or load capacities from instantaneous reserves that are available in the electricity market for that situation. They are divided in fast instantaneous reserve and sustained instantaneous reserve and have the purpose of recovering the system frequency to its nominal values within specific time frames for each type of reserve.

Due to its topology, the primary frequency control does not restore the frequency to pre-disturbance values and, therefore, a secondary frequency control is needed. In New Zealand, this is done by the multiple frequency keeping (MFK) service. MFK is an ancillary service that is used to correct frequency and system errors [8]. It adjusts the real power output and sets the error between the measured frequency and 50Hz to zero [9].

B. Inertia and Rate of Change of Inertia (RoCoF)

Before the action of the governor control, frequency keeping and instantaneous reserve deployments during contingencies in power systems, the first natural reaction of a synchronous generator is the inertia response. It is the response related to the stored kinetic energy in its rotational mass. Derivative of rotor frequency can be related to power deviation to determine the system inertia (*H*) as depicted in (1) [10, 11].

$$\frac{d\omega}{dt} = \frac{\omega\,(P_m - P_e)}{2HS} \tag{1}$$

Equation (1) shows that *H* and RoCoF are inversely related. With an increase in the system inertia, RoCoF will decrease and vice versa. However, a system with low inertia will have a high RoCoF and will become more susceptible to frequency disruptions. Frequency nadir will reach a point lower than the regular case and can lead to load-shedding and, for worst scenarios, outages [12].

The generator to load frequency deviation representation in s-domain is therefore provided in (2). The related block diagram of (2) is given in Fig. 1.

$$\Delta\omega(s) = \frac{1}{2Hs + D}\left[\Delta P_m(s) - \Delta P_L(s)\right] \tag{2}$$

where ΔP_m is change in mechanical power input, ΔP_L are change in loads that are not sensible to frequency change, D is the load-damping constant, $\Delta\omega$ is frequency deviation and H is the inertia constant.

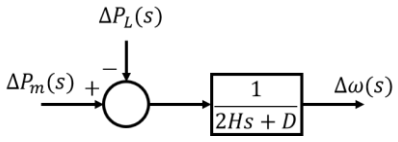

Fig. 1: Generator and load block diagram [13]

A power system with hydro, thermal and nuclear power plants with large synchronous generators has naturally a high overall inertia due to the stored kinetic energy inside the rotational mass of those machines. In addition, the more synchronous generators the system has, the more inertia value it will have. New Zealand power system, for instance, is relatively small and operates isolated from other power systems. Thus, it has low inertia and is amenable to frequency disturbances [14].

C. Virtual/Synthetic inertia

A solution for the low inertia problem with high penetration of non-dispatchable RES is the virtual/synthetic inertia approach. Virtual inertia can be described as an emulation of a natural inertia response of synchronous generators through a combination of control algorithms and power electronics integrated with the distributed generation sources and energy storage systems [12]. There are several different virtual inertia topologies. The one used in this research is the derivative control based virtual inertia [15] as given in Fig. 2.

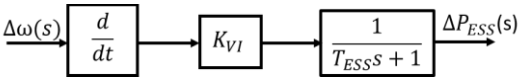

Fig. II: Derivative control based virtual inertia

The output emulated power ΔP_{ESS} of the virtual inertia presented in Fig. 2 is described by **Error! Reference source not found.**.

$$\Delta P_{ESS} = \left[\frac{1}{T_{ESS}s + 1}\right]\left[K_{VI}\left(\frac{d\Delta\omega}{dt}\right)\right] \tag{3}$$

where $\Delta\omega$ is the measured grid frequency deviation, T_{ESS} is the time constant, K_D is the damping coefficient, K_{VI} is the control gain and $\frac{d\Delta\omega}{dt}$ is the rate of frequency deviation.

D. Governor and Turbine Representation

The prime mover model used in this research is the ideal lossless hydro turbine. The turbine mechanical power output changes in response to a change in the gate opening [11]. The transfer function is represented in **Error! Reference source not found.**.

$$\Delta P_m(s) = \frac{1 - \tau_w s}{1 + \frac{1}{2}\tau_w s}\Delta P_{gate}(s) \tag{4}$$

where $\Delta P_{gate}(s)$ represents the change in gate position and τ_w is the water starting time. It is defined as the required time for the water flow from the reservoir to the gate to reach a certain speed [11].

The governor, which in turn controls the opening/closing of the gate can be shown by the s-domain in **Error! Reference source not found.** [13].

$$\Delta P_{gate}(s) = \frac{1}{1 + \tau_g s}\Delta P_g(s) \tag{5}$$

where $\Delta P_g(s)$ is the governor command and τ_g is the time constant. The primary frequency control or governor response with droop is given in **Error! Reference source not found.** [11, 13].

$$\Delta P_g(s) = \Delta P_{ref}(s) - \frac{1}{R}\Delta\omega(s) \quad (6)$$

where ΔP_{ref} is the reference set power and R is the speed regulation. Ref. [11] introduces a transfer function (7) that solves a problem introduced by water inertia opposing initial turbine power change.

$$G_c(s) = \frac{1 + \tau_R s}{1 + \left(\frac{R_T}{R_P}\right)\tau_R s} \quad (7)$$

where τ_R is the reset time, R_T is the temporary droop and R_P is the permanent droop. Combining equations **Error! Reference source not found.** to **Error! Reference source not found.**, a model represented by the block diagram in Fig. 3, which represents a hydro power generator, is obtained.

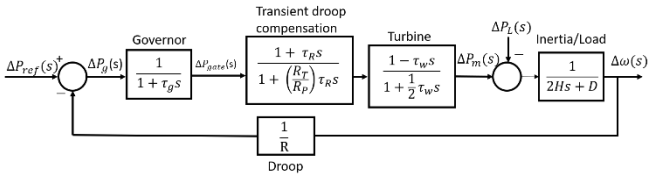

Fig.3: Block diagram of a hydro power generator

E. Primary and Secondary Frequency Control

The governor response is insufficient to bring the network frequency back to its initial value after a disturbance. Generally, the secondary frequency control is an integrator dynamic controller, depicted by $\left[\frac{K_i}{s}\right]$. It receives the frequency deviation signal from the system and sends it to the primary frequency control loop for frequency regulation.

An electrical power system consists of one, two or several control areas. As described, an isolated power system is generally represented as single control area. This research focus on a two-area control system. As commonly presented in the literature, the two-control area system is represented by the two isolated control areas interconnected via an AC tie-line, as of **Error! Reference source not found.** 4 following the equations **Error! Reference source not found.** and **Error! Reference source not found.**. The 1 and 2 indexes (i) on the parameters refers for each area separately.

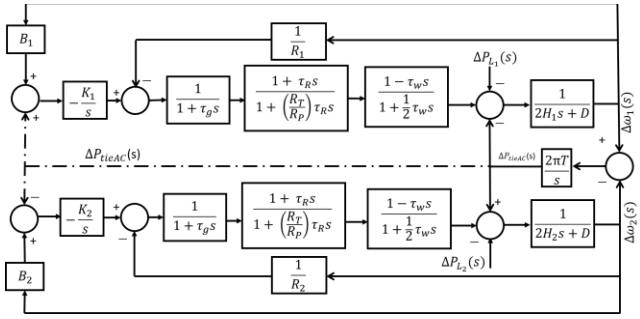

Fig. 4: AGC of a two-area control system

$$\Delta P_{tieAC}(s) = \frac{2\pi T}{s}[\Delta\omega_1(s) - \Delta\omega_2(s)] \quad (8)$$

$$T = \frac{V_1 V_2}{X_{tie}}\cos(\delta_{10} - \delta_{20}) \quad (9)$$

where P_{tieAC} is the real power flow transferred between the areas, ΔP_{tieAC} is the small deviation from the nominal P_{tie} value, X_{tie} is the reactance of the tie, V_1 and V_2 are the voltages at the generator's terminals, δ_{10} and δ_{20} are the nominal phase angles of the voltages V_1 and V_2.

The model of Fig 4 shows a concept called automatic control error (ACE). For an interconnected power system, ACE is a function of the frequency deviation in each area and the delta tie-line, as expressed by (10).

$$ACE_i = B_i\, x\, \Delta\omega_i + \Delta P_{tieAC} \quad (10)$$

where B_i is the bias factor and is commonly determined via natural characteristics of the area [16]. However, the two-area control model with AC tie-line is not consistent for the analysis of this research, as the connection between the two control areas is via HVDC link. Therefore, a dc tie-line interconnection must be represented. Ref. [17] provides the dc-line as a time delay with gain transfer function as shown in **Error! Reference source not found.**.

$$\Delta P_{tieDC}(s) = \frac{K_{dc}}{1 + sT_{dc}}[\Delta\omega_1(s) - \Delta\omega_2(s)] \quad (11)$$

where K_{dc} is the gain, T_{dc} is the settling time of dc current after a load imbalance and ΔP_{tieDC} is the small disturbance from the nominal dc power flow in the DC tine-line.

Equation **Error! Reference source not found.** is still not accurate for the proposed model. The HVDC link between the two control areas participates in the load frequency control via its own controller called frequency keeping control (FKC). It helps diminishing the frequency nadir by reducing de frequency difference between the two islands $[\Delta\omega_1(s) - \Delta\omega_2(s)]$. The dc tie-line and FKC to be used in the model, respectively, are as given in (12) and (13).

$$\Delta P_{tieDC}(s) = \left[\frac{1}{0.25s + 1}\right]\left[\frac{1}{15s} + 250\right][\Delta\omega_1(s) - \Delta\omega_2(s)] \quad (12)$$

$$FKC(s) = \left[\frac{1}{0.25s + 1}\right]\left[\frac{1}{15s} + 250\right] \quad (13)$$

III. PROPOSED METHODOLOGY AND MODELLING

A coherent load frequency control diagram for power systems is designed to propose future methods of frequency controls as they deem necessary. Therefore, the usage of droop and load damping based on the demand is mandatory. In addition, the correct modelling of the MFK and the FKC are extremely important due to their role in maintaining the frequency within the nominal band.

After the modelling of the system, a disturbance should be applied, as to put the system into testing. The step input switching four times an hour has to be applied for testing purposes. Later, to include the penetration of non-dispatchable energy sources as solar and wind, the inertia and droop values of the system will be reduced by 50% and the same simulation will be done. The frequency disruption value will be then analysed. Furthermore, the system will compare the frequency variation and the inclusion of the virtual inertia via ESS in the system. The flowchart for the proposed method in Fig explains this methodology process.

The proposed model for this approach is shown in Fig. 6. This model is based on the control block diagram in [18] and consist of the following main components: The North and South Island power systems, the FKC controller at the HVDC link and the MFK ancillary services. In the model of this research, however, the MFK controller is elaborated, and includes the 30 min timescale of actuation. In addition, the primer mover model from [18], with time constant of 80s [9, 18], is substituted by the hydro generator in Fig. 3, which respond when the frequency varies close to the normal band frequency [8]. Because the thermal units have dead bands of +/- 0.2Hz [18], which are exactly the same as the normal frequency thresholds, they are not included in the model. Moreover, the FKC was included in the model with detail, as it was mathematically described in **Error! Reference source not found.**.

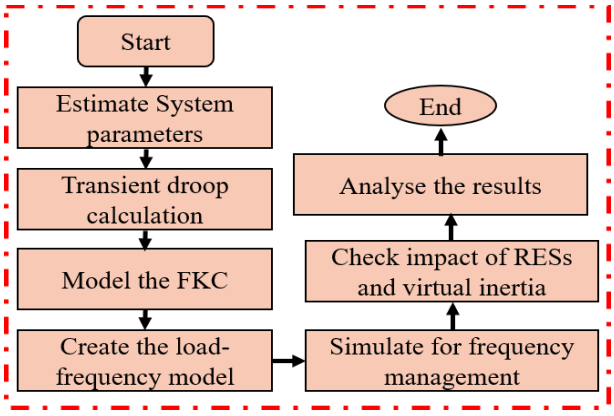

Fig. 5: Flowchart of the methodology

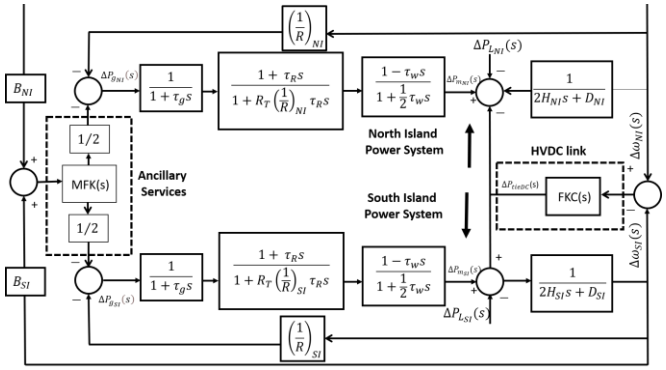

Fig. 6: Two-area LFC model of New Zealand power system

The model of Fig 6 presents a two-area load frequency control model of a New Zealand power system. Each island represents one control area, where the index NI and SI represents North and South Islands, respectively. In addition, there is only one secondary frequency control working for both islands, represented by the MFK. This means that in case of a load imbalance and thus frequency imbalance in one island, the hydro generating units from the other area can also assist in controlling the frequency deviation of the area.

The inputs of MFK are the frequency deviations from both islands, multiplied by its bias factor ($B_{NI} \times \Delta\omega_{NI} + B_{SI} \times \Delta\omega_{SI}$). The Bias factor for both island has the value of 1/2 [18]. The outputs of MFK are divided by two before reaching the governors of each control area. This is because the simulations to be presented in section IV are step inputs of 30MW. As the MFK provision has a limit of 15MW for each island, the output value of MFK (30MW) is then multiplied by a 1/2 factor (depicted as 1/2 blocks in Fig).

The equations that represents the model are shown in (14) to (18).

$$\left[-\left(\frac{1}{R}\right)_{NI}\Delta\omega_{NI}(s)\right]-[\Delta\omega_{NI}+\Delta\omega_{SI}]\frac{1}{s}=\Delta P_{g_{NI}}(s) \quad (14)$$

$$\left[-\left(\frac{1}{R}\right)_{SI}\Delta\omega_{SI}(s)\right]-[\Delta\omega_{NI}+\Delta\omega_{SI}]\frac{1}{s}=\Delta P_{g_{SI}}(s) \quad (15)$$

$$[\Delta P_{m_{NI}}(s)-\Delta P_{L_{NI}}(s)-\Delta P_{tieDC}(s)]\left[\frac{1}{2H_{NI}s+D_{NI}}\right]=\Delta\omega_{NI}(s) \quad (16)$$

$$[\Delta P_{m_{SI}}(s)-\Delta P_{L_{SI}}(s)+\Delta P_{tieDC}(s)]\left[\frac{1}{2H_{SI}s+D_{SI}}\right]=\Delta\omega_{SI}(s) \quad (17)$$

$$\Delta P_{tieDC}(s)=[FKC(s)][\Delta\omega_{NI}(s)-\Delta\omega_{SI}(s)] \quad (18)$$

Equations **Error! Reference source not found.** and **Error! Reference source not found.** show that the governor commands $\Delta P_{g_{NI}}(s)$ and $\Delta P_{g_{SI}}(s)$ are dependent on primary and secondary controls. If the MFK(s) is not actuating, only the primary frequency control will respond to a load disturbance. Equations **Error! Reference source not found.** and **Error! Reference source not found.**, on the other hand, are based on (2). The major difference is related to the actuation of FKC controller through $\Delta P_{tieDC}(s)$. FKC frequency control is shown by (18). It is a controller that has the purpose of minimising the absolute frequency difference between the two islands $\Delta\omega_{NI}(s)-\Delta\omega_{SI}(s)$ [19].FKC(s) is represented in (13).

IV. SIMULATIONS

The model of Fig is built in the MATLAB/Simulink with all the controllers. The model was created using mostly the transfer function blocks, called "Transfer Fcn". The limits are designed using the "Saturation" and "DeadZone" blocks. Moreover, the PI(s) controller is done by using the "PID controller" block and choosing the option PI controller. However, more attention is needed to emulate the MFK ancillary service as presented in Fig. To simulate the model, the parameters in Table I are used.

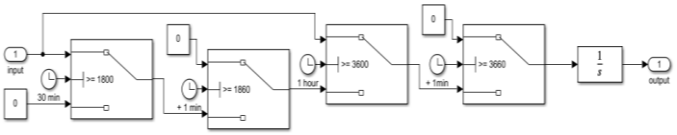

Fig. 7: MKF design on MATLAB/Simulink

The clock block represents the time of the simulation and the block with "0" is a constant block with zero value. The first switch (from left to right) starts at zero. Within 30 minutes (1800 seconds) the switch changes its position from zero to the actual input (see (14) and (15)) . The second switch keeps the integrator on the system for 1 minute and switch backs to zero. The third switch has the same action as of the first one. Later, the fourth switch minute removes the integrator of the system after 1.

When the position of the switch is at zero, there is no actuation of the controller, as the integrator receives a zero value as input. After 30 minutes and 1 hour, the integrator actuates and stays on the system for 1 minutes, as to mimic the procurement of the ancillary service by the system operator.

Simulation case I describes the frequency response to the load switching at each island with and without the MFK

ancillary service as depicted in Fig. 8 and Fig. 9. Furthermore, a comparison of the frequency responses for each island is presented. It has the purpose of showing that the system can operate without the MFK for a certain period. However, the frequency error increases over time and the actuation of the ancillary service is therefore needed.

Simulation case II has the purpose of considering the inclusion of non-dispatchable renewable energy sources as presented in Fig. 10 and Fig. 11. This is done by reducing the inertia and droop control by 50%, as to consider a future worst-case scenario, where several synchronous generators will be out of the system and the no-inertia generating units will be online. This can happen through the middle of the day, where the number of solar panels in the system will surpass the number of online synchronous generators. Updating the droop and inertia values of the system, the same load switches are executed.

Simulation case III on the other hand represents the impact of the virtual inertia in the frequency control and compared without the impact of virtual inertia as deployed in Fig. 10 and Fig. 11. This is done by considering that most of the future residential PV systems will be installed with ESS and that those ESS will be used to emulate inertia. Therefore, the frequency response of each island for the load switches with MFK and virtual inertia in a 50% less inertia and droop will be analysed.

TABLE I. PARAMETERS

Parameters used in the simulation						
Parameter	H_{NI}	H_{SI}	$(1/R)_{NI}$	$(1/R)_{SI}$	D_{NI}	D_{SI}
Value	4.74s	2.85s	7.79pu	20.02pu	0.77pu	0.44pu
Parameter	τ_ω	τ_R	T_{ESS}	K_{VI}	τ_g	*Bias*
Value	2.0s	9s	10s	15	0.5s	0.5

Simulation case I: 30MW load switching comparison with and without MFK

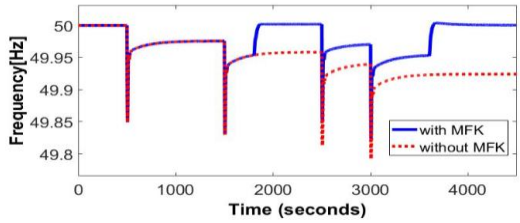

Fig. 8: Frequency response in North Island – with and without MFK

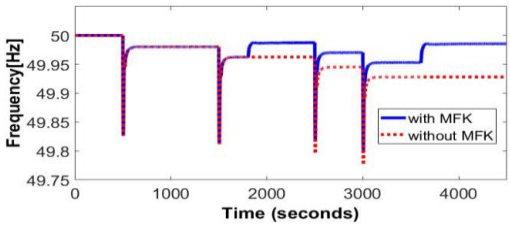

Fig. 9: Frequency response in South Island – with and without MFK

Simulation case II & III: 30MW load switching with decrease of 50% in inertia and droop values as well as actuation of MFK and impact of virtual inertia

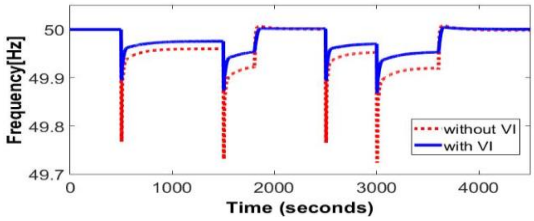

Fig.10: Frequency response in North Island (low inertia condition) – with and without virtual inertia

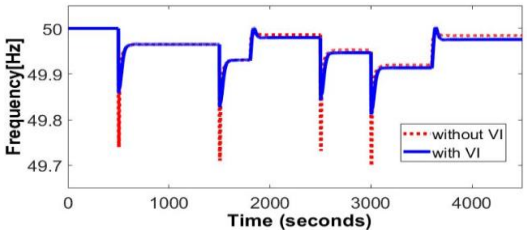

Fig. 11: Frequency response in South Island (low inertia condition) – with and without virtual inertia

Table II shows the summary of the results in the presented simulation cases.

TABLE II. RESULTS

Simulation of 30MW load switches				
	North Island		***South Island***	
System condition	Freq. nadir	Freq. error	Freq. nadir	Freq. error
without MFK	49.79Hz	76mHz	49.78Hz	71.9mHz
with MFK	49.82Hz	0.5mHz	49.8Hz	14.6mHz
low inertia without virtual inertia	49.72Hz	1.6mHz	49.70Hz	15.6mHz
low inertia with virtual inertia	49.87Hz	0.52mHz	49.81Hz	24.3mHz

V. RESULTS AND DISCUSSION

As discussed in Section IV, New Zealand frequency management as a case study can be represented as a two-area load frequency control model. The frequency management, executed by the system operator, is represented by the MFK transfer function and the load switches within the proposed model. The North and South Islands are considered as two different control areas connected by a dc-tie line that is the HVDC link. FKC is one of the frequency controllers included in the system. The values of inertia, droop and load-damping used in this research model are the actual average values from New Zealand power system. Moreover, the other constants used were assumed the most common used in these types of studies.

As observed in Section IV, the proposed model responds coherently with the reality of a real-time operation. The frequency drops due to a decrease in load. The frequency nadir reaches lower values as the overall inertia of the system decreases. The simulation without the ancillary service shows clearly the accumulated frequency error of the system caused by the load switching, responded only by the actuation of the droop controls. The need for the MFK ancillary service is thus verified, and its performance is analysed. The frequency error reaches values very close to zero and the frequency nadir increases from 49.79Hz to 49.82Hz in the North Island and from 49.78Hz to 49.80Hz in the South Island as presented in

Table II. Those increases bring the frequency value to the normal band.

The usage of energy storage system of PV systems can be added to the load frequency model to support the load frequency control in a low inertia condition. This was confirmed by the usage of the ESS's to emulate inertia with the combination of control methods. The selected controller was based on a derivative control-based topology, and the graphs of Fig 10 and Fig 13 confirm its efficacy. In detail from Table II, the frequency nadir increases from 49.72Hz to 49.87Hz in the North Island and from 49.70Hz to 49.81Hz in the South Island.

The proposed model behaves as expected. Initially, as stated by [11], the system frequency is dependent on active power balance. Thus, a change in active power demand is reflected by a change in the system's frequency. This clearly happens with the model as the variation of $\Delta P_{L_{NI}}(s)$ or $\Delta P_{L_{SI}}(s)$ results in a variation of frequency as represented by $\Delta\omega_{NI}(s)$ and $\Delta\omega_{SI}(s)$, respectively.

$\Delta P_{L_{NI}}(s)$ and $\Delta P_{L_{SI}}(s)$ are step load changes that may cause frequency deviation. Therefore, the integral control needs to be actuated to minimize the steady state frequency error. As described in [20], the integrator output increases as long as an error remains and, therefore, causes the rotor to change its speed. The integrator output and, thus, the speed changer position will reach a constant value only when the frequency error is reduced to zero. The MFK actuation on the system is represented by the actuation of the integral controller.

The impact of solar and wind in the system is represented by a decrease in the overall inertia of the system. This statement is reasonable as there is a prospect of substitution of thermal power plants by wind power plant in New Zealand, which means that the overall inertia of the system will be reduced. For solar PV systems, the system inertia reduction happens due to specific scenarios of the day. For example, there will be more solar power in the system during clear afternoon day. It is important to mention that the case scenario of inertia reduction to 50% is just an example and it does not represent the actual New Zealand power system condition. The decrease in overall inertia leads to an increase in the RoCoF, which causes the frequency nadir to reach lower values. However, the virtual inertia controller compensates for the low inertia and increases the frequency nadir to be within the normal operation limit.

VI. CONCLUSION AND FUTURE WORK

This research has proposed a load frequency control model for small power systems with two control area using a New Zealand power system as a case study. The results show that the proposed technique is coherent in keeping the frequency of the system within the normal band under system disturbances. The research has also investigated the effects of RESs penetration to the grid and the use of virtual inertia to mitigate the effect of low system inertia. The combination of the proposed load frequency control with virtual inertia works well to safeguard frequency stability even in systems with high penetration of RESs.

As a future work for this research, it is important to take further research of the time-varying inertia in power system as the penetration of stochastic RESs keep increasing in power systems. Furthermore, there should be an investigation of alternative frequency controllers as back-up in case of FKC failure.

REFERENCE

[1] B. Harker and K. Gibbs, "Frequency Control on the New Zealand Power System," in *IPENZ Annual Conference 1989*. Institution of Professional Engineers New Zealand, p. 498.

[2] A. Fathi, Q. Shafiee, and H. Bevrani, "Robust Frequency Control of Microgrids Using an Extended Virtual Synchronous Generator," 2018.

[3] M. Woods. Transitioning to more affordable and renewable energy: The energy markets work programme [Online] Available: https://www.mbie.govt.nz/dmsdocument/5960-transitioning-to-more-affordable-and-renewable-energy-the-energy-markets-work-programme-proactiverelease-pdf

[4] C. M. Blair Walter. Wind energy to be 20% of nz generation by 2035 [Online] Available: http://www.windenergy.org.nz/20-of-nz-generation-by-2030

[5] E. a. I. Markets, "Energy in New Zealand," Wellington New Zealand. [Online]. Available: https://www.mbie.govt.nz/dmsdocument/7040-energy-in-new-zealand-2019

[6] Transpower. Power system live data [Online] Available: https://www.transpower.co.nz/power-system-live-data

[7] M. Pelletier, M. Phethean, and S. Nutt, "Grid code requirements for artificial inertia control systems in the New Zealand power system," in *2012 IEEE Power and Energy Society General Meeting*, 2012: IEEE, pp. 1-7.

[8] L. Meng *et al.*, "Fast Frequency Response From Energy Storage Systems—A Review of Grid Standards, Projects and Technical Issues," *IEEE Trans. on Smart Grid*, vol. 11, no. 2, pp. 1566-1581, 2019.

[9] J. Schipper, A. Wood, C. Edwards, and A. Miller, "Recommendations for Ancillary Service Markets under High Penetrations of Wind Generation in New Zealand," 2019.

[10] T. Kerdphol, F. S. Rahman, Y. Mitani, M. Watanabe, and S. Küfeoğlu, "Robust virtual inertia control of an islanded microgrid considering high penetration of renewable energy," *IEEE Access*, vol. 6, pp. 625-636, 2018.

[11] P. Kundur, N. J. Balu, and M. G. Lauby, *Power system stability and control*. McGraw-hill New York, 1994.

[12] T. Ujjwol, S. Dipesh, M. Manisha, P. B. Bishnu, M. H. Timothy, and T. Reinaldo, "Virtual Inertia: Current Trends and Future Directions," *Applied Sciences, Vol 7, Iss 7, 2017*.

[13] H. Saadat, "Power System Analysis Third Edition. United State America: Victor Graphic," ed: Inc, 2010.

[14] N.-M. Vong, S. Pillay, and V. Lo, "Effect of solar PV on frequency management in New Zealand," in *2017 IEEE Innovative Smart Grid Technologies-Asia (ISGT-Asia)*, 2017: IEEE, pp. 1-6.

[15] E. Rakhshani, D. Remon, A. M. Cantarellas, and P. Rodriguez, "Analysis of derivative control based virtual inertia in multi-area high-voltage direct current interconnected power systems," *IET Generation, Transmission & Distribution*, vol. 10, no. 6, pp. 1458-1469, 2016.

[16] M. Camponogara and D. P. Bernardon, "Evaluation of Automatic Generation Control Modes Using ANATEM Software," in *2019 IEEE PES Innovative Smart Grid Technologies Conference-Latin America (ISGT Latin America)*, 2019: IEEE, pp. 1-5.

[17] A. Prakash, K. Kumar, and S. Parida, "A novel I-PDF controller for LFC with AC/DC Tie-line," in *2019 20th International Conference on Intelligent System Application to Power Systems (ISAP)*, 2019: IEEE, pp. 1-6.

[18] J. Schipper, A. Wood, A. Miller, and C. Edwards, "The Value of Frequency Keeping and Governor Response to New Zealand," 2016.

[19] S. P. Teeuwsen, G. Love, and R. Sherry, "1400 MW New Zealand HVDC upgrade: Introducing power modulation controls and round power mode," in *2013 IEEE Power & Energy Society General Meeting*, 2013: IEEE, pp. 1-5.
[20] O. I. Elgerd, "Electric energy systems theory: an introduction," 1982.